Thin Solid Films 594 (2015) 156–161

Contents lists available at ScienceDirect

Thin Solid Films

journal homepage: www.elsevier.com/locate/tsf

Modeling thermal stress in thin films produced by photonic curing

Martin J. Guillot

Department of Mechanical Engineering, University of New Orleans, New Orleans, LA 70148, USA

ARTICLE INFO

Article history:
Received 16 July 2015
Received in revised form 3 October 2015
Accepted 5 October 2015
Available online 8 October 2015

Keywords:
Thermal stress model
Thin film
Photonic curing
Transient temperature variation
Flexible electronics

ABSTRACT

A thermal stress model is developed to simulate stresses produced in the processing of thin film metal inks due to arbitrary time dependent temperature variations through the film stack. The current model employs and extends the method developed by Hsueh (2002), which models stresses in thin films where the temperature of each layer in the film stack was assumed to be uniform at a temperature different from the initial temperature. The model results in two integrals involving temperature distribution through the film stack. The thermal stress model developed is validated using two cases where analytical temperature solutions are available. The first is a constant surface heat flux on a single layer. The second is a constant surface temperature on a three-layer film stack. Both cases begin from an initial uniform temperature. The integrals appearing in the expressions for stress distributions are computed using the analytical solutions of the temperature distributions and are used to compute the stress distributions through the film stack. The analytical solutions are compared to numerical results produced by solving the transient heat conduction equation using a previously developed finite volume method. In the numerical solutions, the integrals involving temperature are approximated using the midpoint rule. The computed numerical results compare very well with the analytical solutions for both cases studied.

1. Introduction

Thin multilayered films have a wide range of applications, including solid-state electronics, composite laminated protective coatings, and flexible electronics [1]. Flexible electronic applications have grown to include RFID tags, large-area displays, and photovoltaics, among others. Applications currently under development include wearable sensors, "smart" clothing, and flexible cell phones and tablets that allow users greater degrees of freedom to interact with mobile devices. Suganuma [2] presents a summary of many of the current manufacturing methods used to develop flexible electronic circuits for a wide range of applications, and discusses the advantages and disadvantages of each method. The market for flexible electronics will continue to expand as the demand for robust mobile electronics continues to grow, so the need for inexpensive and rapid techniques for the manufacture and thermal processing of thin film metallic inks to form flexible electronic circuits will become more critical.

One method for manufacturing flexible electronic circuits involves using an ink jet printer to print circuits made from nanoparticle copper or silver suspended in binders and solvents onto inexpensive flexible substrates such as polyethylene terephthalate (PET) or paper. The inks must then be dried and sintered to make them highly conductive. A bottleneck in the manufacturing of printed electronics has been the thermal processing of the inks. The thermal processing time is reduced exponentially with increased processing temperature, so the highest temperature possible is typically used. With traditional sintering methods that bring the ink and substrate into thermal equilibrium, such as ovens or infrared heaters, this temperature is most often limited by the substrate. Expensive substrates typically have higher maximum working temperatures, but inexpensive substrates such as PET have a maximum working temperature around 150 °C, so traditional methods are limited below these temperatures. This limitation forces a long processing time—often minutes, which means that production is limited by oven size. A thin-film processing technology termed "photonic curing" [3–4] uses repeated short pulses (on the order of hundreds of microseconds) from xenon flashlamps to heat the film to sintering temperature without damaging the substrate. A typical copper-based ink pattern on paper is shown in Fig. 1 before and after sintering with photonic curing. The pulsed light produced during photonic curing produces a time-varying heat flux that can act as a surface heat flux or a volumetric heat source, depending on the absorption properties of the materials. The short-pulse radiant heating makes it possible to heat a thin film on a low-temperature substrate to a temperature far beyond the substrate's maximum working temperature using methods that bring the film and substrate into thermal equilibrium. Coupled with roll-to-roll processing, photonic curing facilitates rapid and efficient processing of thin film metal inks.

Thermal stresses are produced during the thermal processing of the film stack. Traditional sintering methods, such as ovens, that bring entire film stack into thermal equilibrium at a temperature different from the initial deposition temperature produce thermal stresses due solely to each material having different coefficients of thermal expansion— that is, CTE mismatch between layers. With photonic

E-mail address: mjguillo@uno.edu.

http://dx.doi.org/10.1016/j.tsf.2015.10.012
0040-6090/

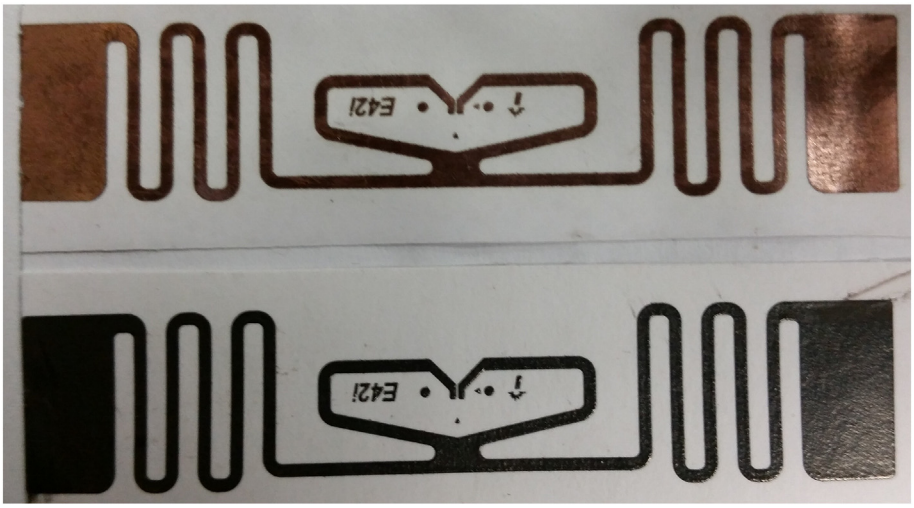

Fig. 1. Typical copper based ink circuit pattern on paper.

curing, time-dependent temperature variations through the film stack occur due to the pulsed energy cycling of the xenon flashlamps. This produces thermal stresses due to nonuniform temperature in the film stack as well as CTE mismatch.

The response of single-material and multimaterial films and strips to thermal variations in their cross sections has been of interest even before Timoshenko derived an analytical solution for a bimetal strip subjected to uniform heating from an initial temperature in 1925 [5]. Timoshenko summed forces and moments in each layer and imposed strain continuity at the interface to develop an analytical solution for stress and displacement of the strip. Since then, many researchers have developed methods to model thermal stresses in thin films using various approximations. Many of the earlier works built on the work of Timoshenko by summing forces and moments and imposing interface strain compatibility to develop a system of $2N + 1$ equations for an N-layer composite. The solution was a set of N forces and N moments that summed to zero (for unconstrained layers), and the radius of curvature of the stack. For a single layer Boley and Weiner [6] present the analytical solution for an unconstrained plate with arbitrary temperature variation through the thickness. Olsen and Ettenberg [7] and Shimizu et al. [8] developed a stress model for multilayer composites assuming the entire stack to be at a uniform temperature different from the initial temperature, so the resulting stresses were due solely to CTE mismatch. Feng and Liu [9] and Liu and Murarka [10] generalized the method to allow for temperature differences between layers, but each layer was assumed to be at a uniform temperature. Lu and Fleck [11] developed a model to study thermal shock resistance of a single-layer solid. The stress model was coupled to a 1-D transient heat conduction model. Malzbender and Steinbrech [12] used bending methods to determine mechanical properties in single-layer and multilayered materials, and Malzbender [13] used the results of this work to develop a model for elastic deformation in multilayered materials due to external loads and moments and CTE mismatch between layers. Zhang et al. [14–15] developed models based on summing forces and moments to study thermally induced stresses in multilayer coatings that included graded material properties and compositions where the stresses were due solely to thermal mismatch strain. Evans and Hutchinson [16] studied the delamination mechanics of oxide coatings in thermal gradients of aero-turbine engines. The authors considered steady-state and transient temperature gradients in three-layer coating systems. More recently, researchers have developed models for thermal stress that reduce the number of unknowns from $2N + 1$ to three or less. Freund [17–18] developed a model for stress distribution in an unconstrained heteroepitaxial layer in terms of the location where the epitaxial mismatch strain is zero and the curvature of the layer at that plane. It was assumed that the epitaxial strain was known. Giannakopolous et al. [19] extended the method to constrained layers where external forces and moments are applied. Following the approaches of Freund and Giannakopolous, Hsueh [20] developed a more generally applicable method for computing stresses in thin films that reduced the number of unknowns to three and was not restricted to epitaxial layers where the epitaxial mismatch strain is known. Hsueh, however, assumed that the entire film stack was heated uniformly and that the resulting stresses were due solely to CTE mismatch between layers. The resulting stress was written in terms of a uniform strain, a bending strain, and the location of the bending axis, where the bending axis was defined as the location where the bending strain was zero (as opposed to the customary "neutral axis", which is defined as the location where the normal stress is zero). Zhang [21] developed an alternative two-variable formulation, also assuming uniform temperature throughout the stack. Both Hsueh and Zhang separate film and substrate in the nomenclature of their expressions, although this is not necessary. The substrate is simply another layer in the stack. Feng et al. [22] developed a model for stresses in circular thin films subjected to nonuniform steady-state temperature distributions. Sundaram et al. [23] investigated the effect of transient thermal gradients on delamination of thermal barrier coatings.

This work applies and extends Hsueh's analysis to allow for a time-dependent thermal profile throughout the film stack to compute thermal stresses in thin films exposed to the time-dependent heat flux encountered in photonic curing. The resulting expression for stress distribution is analytical and involves integrals of the temperature distribution within the film stack. The objective is to incorporate the thermal stress model into the finite volume discretization of the transient heat conduction equation and validate it by comparing the numerically computed results to two cases where analytical solutions are available. The two cases are a single-layer model subject to constant heat flux and a three-layer model subject to a constant temperature on the top boundary.

2. Thermal stress model

A transient thermal simulation model was previously developed and validated by Guillot et al. [24–25] and used to simulate photonic curing. The thermal-simulation model couples a finite volume discretization of the heat-conduction equation to a graphical user interface written in LabView and a database of thermally dependent material properties to

which the user can add user-defined materials. The geometric, material, and pulse parameters are all specified using the interface. The output is a graphical time–temperature history at all locations within the stack that are viewable within the same interface. Complete details of the finite volume development are presented in [25].

Consider a multiple-layer material, as shown in Fig. 2, initially assumed to be stress free at a uniform temperature T_o and then subjected to temporally varying heat flux that produces a time-dependent temperature variation through its depth. The temperature variation produces thermal strains and corresponding stresses due to the variation in temperature and the CTE mismatch between layers. Hsueh [20] proposed that the total strain could be written as a sum of a uniform component and a bending component:

$$\varepsilon = c + \frac{(t_b - x)}{r} \qquad 0 \le x \le H, \tag{1}$$

where the first term c is the uniform strain component and the second term is the bending component. The quantity t_b is the location of the bending axis (m), and r is the radius of curvature (m). The total film stack depth is H (m). The origin of the coordinate system is arbitrary, but in this work we place the origin of the coordinate system at the top of the film stack with the positive direction pointing into the stack. The resultant normal stress can be written as.

$$\sigma_{xx}(x,t) = E_i(x)[\varepsilon(x) - \alpha_i(x)\Delta T(x,t)], \tag{2}$$

where E_i (Pa) and α_i (m/m °C) are the modulus of elasticity and the linear CTE, respectively, which are different for each layer and can vary within a layer (e.g., due to temperature variations). The difference in temperature between the current time t and the initial uniform temperature T_o is given by $\Delta T_i(x,t)$. For planar geometries rather than strips, Young's modulus should be replaced by the biaxial modulus $\bar{E} = E/(1-\nu)$, where ν is Poisson's ratio. The stress for a given film-stack composition is completely defined by determining c, t_b, and r.

For unconstrained film stacks, the resultant force and moment on the film stack is zero. This can be written as.

$$\int_0^H \sigma_{xx} dx = 0 \qquad \int_0^H \sigma_{xx}(t_b - x)\ dx = 0. \tag{3}$$

The quantities that determine the stress can be computed sequentially by superposition. Using the first term of Eq. (3), the resultant forces due to the normal strain and the bending strain components are separately set to zero. Then using the second term of Eq. (3), the resultant moment about the bending axis is set to zero. In the following expressions, E_i and α_i are assumed constant within each layer but can vary from layer to layer. The method, however, extends in a straightforward way to cases where those quantities vary within a layer and would result in integrations involving modulus of elasticity and CTE in addition to the integrals involving temperature distribution.

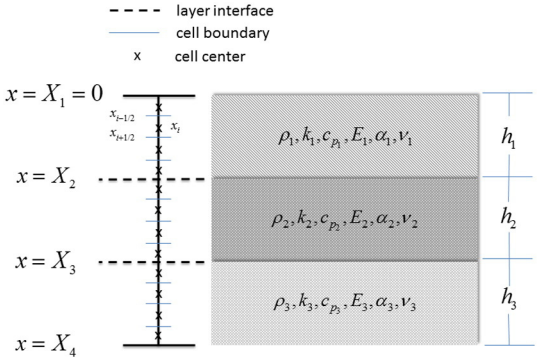

Fig. 2. Typical material stack geometry and cell definitions.

For a film stack composed of N layers, the resultant force due to the uniform strain component can be written as.

$$\sum_{i=1}^{N} \int_{X_i}^{X_{i+1}} E_i(c - \alpha_i \Delta T_i) dx = 0. \tag{4}$$

If the CTE and modulus of elasticity are constant within each layer, then Eq. (4) can be integrated and solved for the uniform strain component c as.

$$c = \frac{\sum_{i=1}^{N} E_i \alpha_i \int_{X_i}^{X_{i+1}} \Delta T_i dx}{\sum_{i=1}^{N} E_i h_i}, \tag{5}$$

where $h_i = X_{i+1} - X_i$ is the thickness of the ith layer. The force due to the bending stress can be written as.

$$\sum_{i=1}^{N} \int_{X_i}^{X_{i+1}} E_i \frac{(t_b - x)}{r} dx = 0. \tag{6}$$

Integrating and solving for t_b gives.

$$t_b = \frac{\sum_{i=1}^{N} E_i h_i (h_i + 2X_i)}{2\sum_{i=1}^{N} E_i h_i}. \tag{7}$$

Note that the location of the bending axis is independent of the temperature and depends only on the stack geometry and material properties. Finally, setting the bending moment to zero gives the radius of curvature of the stack as.

$$\frac{1}{r} = \frac{-\frac{c}{2}\sum_{i=1}^{N} E_i h_i (X_i + X_{i+1}) + \sum_{i=1}^{N} E_i \alpha_i \int_{X_i}^{X_{i+1}} \Delta T_i x\, dx}{\sum_{i=1}^{N} E_i h_i \left[\frac{t_b}{2}(h_i + 2X_i) - \frac{1}{3}(X_i + X_i X_{i+1} + X_{i+1})\right]}. \tag{8}$$

The stress is determined by the thermal and geometric properties of the film stack and the two integrals involving temperature, which are given by.

$$\int_{X_i}^{X_{i+1}} \Delta T_i\, dx \qquad \int_{X_i}^{X_{i+1}} \Delta T_i\, x\, dx. \tag{9}$$

The stress model is a quasi-static model. That is, the stack displacement and radius of curvature at any given time depend only on the geometric and material properties of the stack and the temperature distribution at that time. The time dependency of the stress is solely due to the time dependency of the temperature distribution. The stress distribution described by Eqs. (5), (7), and (8) is purely analytical. If analytical temperature distributions are known and can be integrated via Eq. (9), the resulting stress distributions are analytical. It is easily shown that for a single layer, the stress predicted by Eqs. (1)–(8) reduces to the solution given by Boley and Weiner [6] for a free plate with temperature variation through the thickness.

3. Stress model validation with analytical temperature distributions

The stress model described in the previous section was incorporated into the heat-conduction model. The numerical solutions were compared to the two previously described cases where analytical temperature distributions were known so that the integrals appearing in Eq. (9) could be computed analytically. The resulting analytical stress distributions were compared to the stress distribution computed using the temperature distributions predicted by the finite volume heat-conduction code and approximating the integrals appearing in the stress model using the midpoint rule for each finite volume cell.

3.1. Case 1: single-layer model

The temperature distribution throughout a single layer of material subjected to a uniform heat flux at the top surface can be approximated by a semi-infinite body as long as the duration is short enough that the thermal effects do not reach the bottom boundary. Using the Green's function approach, Beck [26] writes the solution as

$$T(x,t)-T_i=\frac{2\sqrt{at}}{k}q_s''\left(\frac{1}{\pi^{1/2}}\exp\left(-\frac{\xi^2}{4\mathbf{Fo}}\right)-\frac{\xi}{2\mathbf{Fo}^{1/2}}\operatorname{erfc}\left(\frac{\xi}{2\mathbf{Fo}^{1/2}}\right)\right), \tag{10}$$

where a is the thermal diffusivity (m^2/s), k is the thermal conductivity (W/m K), q_s'' is the surface heat flux (W/m^2), H is the depth of the layer (m), $\mathbf{Fo}=(a/H^2)t$, and $\xi=x/H$.

3.2. Case 2: three-layer model

Sun and Wichman [27] develop a temperature solution for a three-layer composite initially at uniform temperature T_o, at $t=0$, with the top boundary at $x=0$ suddenly raised to T_1 for $t>0$. The bottom surface remains fixed at T_o. The authors develop the solution in terms of the following nondimensional variables: $\theta=(T-T_o)/(T_1-T_o)$, $\xi_1=x/h_1$, $\xi_2=(x-h_1)/h_2$, $\xi_3=(x-(h_1+h_2))/h_3$, $\tau=t/t_o$, $\delta_i=\eta_i t_o/h_i^2$, and $\kappa_i=k_i/h_i$, for $i=1,2,3$. The depth of the ith layer is h_i, and t_o is an arbitrary reference time.

The authors decompose the nondimensional temperature solution within each layer into steady and unsteady components. The details of the solution method are given in the reference, and only the results are repeated here for convenience. The solution is written as

$$\theta(\xi_i,\tau)=\psi(\xi_i)-\phi(\xi_i,\tau). \tag{11}$$

The steady solutions within each layer are written as

$$\begin{aligned}\psi&=1-(\Delta\theta)_1\xi_1 \quad \text{in } \xi_1\in(0,,,1)\\ \psi&=1-(\Delta\theta)_1-(\Delta\theta)_2\xi_2 \quad \text{in } \xi_2\in(0,,,1)\\ \psi&=1-(\Delta\theta)_1-(\Delta\theta)_2-(\Delta\theta)_3\xi_3 \quad \text{in } \xi_3\in(0,,,1)\end{aligned}, \tag{12}$$

where $\Delta\theta_i=(1/\kappa_i)/(1/\kappa_1+1/\kappa_2+1/\kappa_3)$.

The unsteady solutions are written as

$$\phi_i(x,t)=\Delta_i\sum_{n=1}^{\infty}A_n e^{-\lambda_n^2\delta_1\tau}\Phi_n^i(\xi_i) \quad \text{in } \xi_i\in(0,,,1) \text{ for } i=1,2,3. \tag{13}$$

Note that in Eq. (13), the subscript on δ in the exponential is 1, not i. The eigenvalues λ_n are found from the roots of

$$\tan(\lambda_n)=-\frac{(\Delta_2\tan(\mu_{1n})+\Delta_3\tan(\mu_{1n}))}{1-\Delta_3/\Delta_2\tan(\mu_{1n})\tan(\mu_{1n})}, \tag{14}$$

and the eigenfunctions are given by

$$\begin{aligned}\Phi_n^1&=\sin(\lambda_n\xi_1)\\ \Phi_n^2&=\alpha_n\sin(\mu_{1n}\xi_2)+\beta_n\cos(\mu_{1n}\xi_2),\\ \Phi_n^3&=\overline{\alpha}_n\sin(\mu_{2n}\xi_3)+\overline{\beta}_n\cos(\mu_{2n}\xi_3)\end{aligned} \tag{15}$$

where the parameters are defined as

$$\begin{aligned}&\mu_{1n}=\sqrt{\delta_1/\delta_2}\lambda_n,\ \ \mu_{2n}=\sqrt{\delta_1/\delta_3}\lambda_n\\ &\Delta_1=1,\ \ \Delta_2=\kappa_1/\kappa_2\sqrt{\delta_2/\delta_1},\ \ \Delta_3=\kappa_1/\kappa_3\sqrt{\delta_3/\delta_1}\\ &\alpha_n=\cos(\lambda_n),\ \ \beta_n=\sin(\lambda_n)/\Delta_2\\ &\overline{\alpha}_n=\cos(\lambda_n)\cos(\mu_{1n})-\sin(\lambda_n)\sin(\mu_{1n})/\Delta_2\\ &\overline{\beta}_n=\cos(\lambda_n)\sin(\mu_{1n})\Delta_2/\Delta_3+\sin(\lambda_n)\cos(\mu_{1n})/\Delta_3\\ &A_n=\kappa_2\kappa_3/(\lambda_n M_n)\\ &M_n=\kappa_2\kappa_3/2+\kappa_1\kappa_3\left(\cos^2(\lambda_n)+\sin^2(\lambda_n)/\Delta_2^2\right)/2+\kappa_1\kappa_2\left(\overline{\alpha}^2{}_n+\overline{\beta}^2{}_n\right)/2\end{aligned} \tag{16}$$

4. Results and discussion

The parameters for the validation were selected to represent photonic curing as much as possible while using analytical solutions. The relevant material properties—the thermal conductivity k, specific heat c_p, densityρ, Young's modulus E, Poisson's ratio ν, and coefficient of thermal expansion CTE—are given in Table 1. The values for copper and silver are found in [28]. The values for GBS and PET vary depending on the manufacturer and exact composition. The values used in this study should be considered typical. For the numerical solutions, each cell was treated as a layer, with $\{X_i,X_{i+1}\}\rightarrow\{x_{i-1/2},x_{i+1/2}\}$ being the boundaries of the cell.

4.1. Case 1: single layer

The single-layer case was composed of 75 μm copper (Cu) and was subjected to a constant incident heat flux, $q''=200$ kW/cm^2. The total simulation time was 3 μs. The mesh was composed of 250 cells; the number of time steps was 1200. The initial temperature was uniform at 25 °C. The previous validation study [25] demonstrated that these mesh and time step parameters were more than sufficient to ensure converged solutions.

The analytical and numerical solutions for temperature and stress at selected times are given in Figs. 3 and 4, respectively. The temperature distribution solution is straightforward. The numerical stress distribution was computed using the model described in this work. The analytical stress distribution was computed using Eqs. (9.5.5) and (9.5.6a), pg. 278, of Boley and Weiner [6]. The integrals given by Eq. (9) were computed using Eq. (10), and the results are presented in Appendix A. It is seen from the figures that the numerical and analytical solutions agree very well. For this case, the layer is in compression near the top and bottom surfaces, while the midsection is in tension. As the sample initially heats, the top surface's compressive stress increases, but the rate of increase slows at later times. The magnitude of the stress continues to increase during the simulation, and the location of the maximum tensile stress travels down the layer. As the magnitude of the tensile stress increases, the magnitude of the compressive stress near the top and bottom surfaces increases to maintain overall force and moment

Table 1
Thermal & mechanical properties of materials in thin film stacks.

Material	k (W/m K)	c_p (J/kg K)	ρ (gm/cm^3)	E (GPa)	ν (−)	CTE (μm/m K)
Cu	401	382.5	8.96	115	0.33	16.6
Ag	420	234.8	10.5	83	0.37	18.9
GBS	1.14	820.0	2.24	64	0.20	3.3
PET	0.24	729.9	1.37	3.5	0.39	59.0

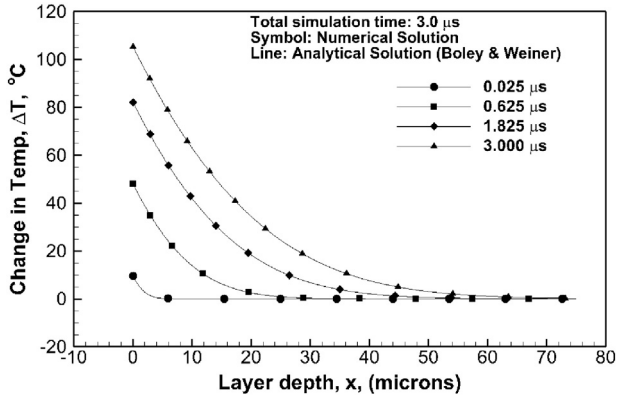

Fig. 3. Single layer model, temperature distribution at select times.

equilibrium. The maximum compressive stress is approximately 110 MPa, and the maximum tensile stress is approximately 50 MPa.

4.2. Case 2: three-layer model

The three-layer case was composed of 1 μm silver (Ag), 5 μm glass borosilicate (GBS), and 100 μm PET. Constant temperature boundary conditions were applied at the top and bottom surfaces. Initially, the stack was at 25 °C uniform temperature. For $t > 0$ the temperature on the upper boundary was raised to 125 °C, while the temperature on the bottom boundary was maintained at 25 °C. The number of cells was 47, 47, and 156 in layers 1, 2, and 3, respectively. The total simulation time was 1.2 ms. This geometry was chosen as representative of typical photonic curing applications involving multilayer film stacks. Due to the complexity of the solution, our implementation of the analytical temperature model was validated by comparing our computed solution to the solution presented by Sun and Wichman in reference [27]. The authors present the first 20 computed eigenvalues and temperature distribution for an example case. We reproduced the table of eigenvalues and the temperature distribution (Table 1 and Fig. 3a in their work, respectively). Having validated our implementation, we then re-solved Eq. (14) for the eigenvalues for our case using the Newton–Raphson iteration method. We computed the first 5000 eigenvalues, which was much more than needed to ensure convergence of the series for the unsteady part of the solution. Having established the accuracy of our implementation of the analytical solution, we then applied the temperature solution to compute the stress using the model developed in this work. The integrals of temperature needed to compute the stress distribution, given by Eq. (9), were computed using the analytical temperature distribution and are presented in Appendix A.

The temperature distributions are shown in Fig. 5 at selected times. The temperature in the first layer is essentially constant. This is

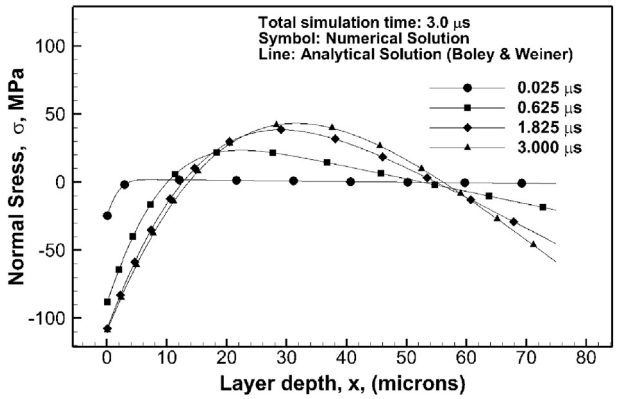

Fig. 4. Single layer model, stress distribution at select times.

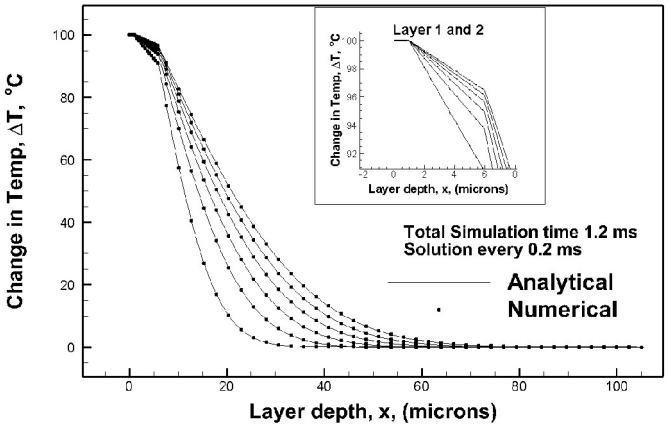

Fig. 5. Three layer model, temperature distribution at select times.

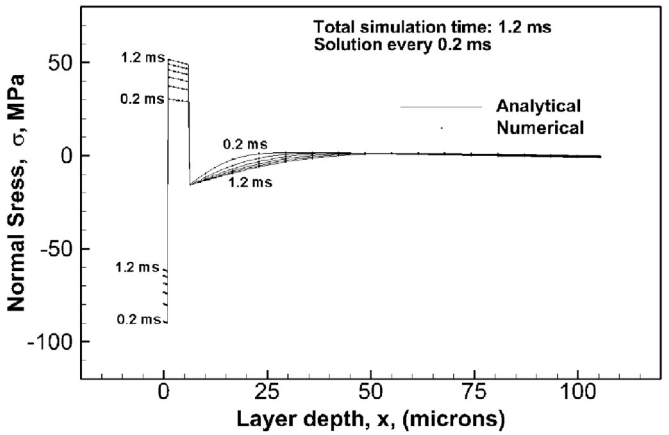

Fig. 6. Three layer model, stress distribution at select times.

expected due to the high conductivity of silver combined with the thinness of the layer. The temperature distribution in the second layer is linear, while the distribution in the third layer varies nonlinearly from the temperature at the interface with layer 2 to the constant temperature on the right boundary.

The normal stress distributions at the same times are shown in Fig. 6. Layer 1 immediately goes into compression, while layer 2 goes into tension. The compression in layer 1 is highest at earlier times (about 120 MPa) and then begins to decrease, whereas the tension in layer 2 is lowest at earlier times and increases with increasing time (up to about 50 MPa). Layer 3 goes into compression up to about the first 20 microns. The compression increases with increasing time to maintain zero net force and moment on the entire stack. After 20 microns, there is slight tension followed by compression toward the lower part of layer 3, with all values in that region being on the order of 1 MPa or less.

5. Conclusions

A thermal stress model based on Hsueh's method was developed and incorporated into a thermal model to simulate the thermal processing of thin films using photonic curing. The model was validated using two cases where analytical solutions were available using film stacks typical of photonic curing. The numerical model agreed very well with the analytical solutions for the two cases studied. The stress model can be used in conjunction with the thermal-simulation model to guide the thermal processing of thin films using photonic curing and to determine optimal parameters that will most efficiently process a given material film stack without causing thermal-related stress damage.

Appendix A

The integrals given by Eq. (9) needed to compute the stress are presented here for the single-layer and three-layer models.

Case 1. Single-layer model

For a single layer of depth H, the temperature integrals become.

$$\int_0^H \Delta T\,dx = \frac{H}{2\pi^{1/2}}\exp\left[\frac{-H^2}{4at}\right] - \frac{H^2}{4\sqrt{at}} + \frac{\left(H^2+2at\right)\operatorname{erf}\left[\frac{H}{2\sqrt{at}}\right]}{4\sqrt{at}}, \tag{17}$$

$$\int_0^H \Delta T x\,dx = -\frac{2at}{3\pi^{1/2}} - \frac{\left(H^2-8at\right)}{24\pi^{1/2}}\exp\left[\frac{-H^2}{4at}\right] + \frac{H\sqrt{at}}{4}\operatorname{erf}\left[\frac{H}{2\sqrt{at}}\right] + \frac{H^3}{24\sqrt{at}}\operatorname{erfc}\left[\frac{H}{2\sqrt{at}}\right]. \tag{18}$$

Case 2. Three-layer model

The integrals appearing in Eqs. (5) and (8), recalling Eqs. (11)–(13), are evaluated as follows:

$$\int_{X_i}^{X_{i+1}} \psi(x)\,dx = \begin{cases} h_1(1-\Delta\theta_1/2) & X_1 \le x \le X_2 \\ h_2(1-\Delta\theta_1-\Delta\theta_2/2) & X_2 \le x \le X_3 \\ h_3(1-\Delta\theta_1-\Delta\theta_2-\Delta\theta_3/2) & X_3 \le x \le X_4 \end{cases}, \tag{19}$$

$$\int_{X_i}^{X_{i+1}} \psi(x)\,x\,dx = \begin{cases} 1/6\,h_1^2(3-2\Delta\theta_1) & X_1 \le x \le X_2 \\ 1/6\,h_2((1-\Delta\theta_1)(6h_1+3h_2)-\Delta\theta_2(3h_1+2h_2)) & X_2 \le x \le X_3 \\ 1/6\,h_3((6(h_1+h_2)+3h_3)(1-\Delta\theta_1-\Delta\theta_2)-\Delta\theta_3(3(h_1+h_2)+2h_3)) & X_3 \le x \le X_4 \end{cases} \tag{20}$$

$$\int_{X_i}^{X_{i+1}} \Phi_n^i(x)\,dx = \begin{cases} h_1(1-\cos(\lambda_n))/\lambda_n & X_1 \le x \le X_2 \\ h_2(\alpha_n-\alpha_n\cos(\mu_{1n})+\beta_n\sin(\mu_{1n}))/\mu_{1n} & X_2 \le x \le X_3 \\ h_2(\overline{\alpha}_n-\overline{\alpha}_n\cos(\mu_{2n})+\overline{\beta}_n\sin(\mu_{2n}))/\mu_{2n} & X_3 \le x \le X_4 \end{cases}, \tag{21}$$

$$\int_{X_i}^{X_{i+1}} \Phi_n^i(x)\,x\,dx = \begin{cases} h_1^2(\sin(\lambda_n)-\cos(\lambda_n))/\lambda_n^2 & X_1 \le x \le X_2 \\ h_2\left(\begin{array}{l} -\beta_n h_2+\alpha_n h_1\mu_{1n} \\ +(\beta_n h_2-\alpha_n(h_1+h_2)\mu_{1n})\cos(\mu_{1n}) \\ +(\alpha_n h_2+\beta_n(h_1+h_2)\mu_{1n})\sin(\mu_{1n}) \end{array}\right)\Big/\mu_{1n}^2 & X_2 \le x \le X_3 \\ h_3\left(\begin{array}{l} -\overline{\beta}_n h_3+\overline{\alpha}_n(h_1+h_2)\mu_{2n} \\ +(\overline{\beta}_n h_3-\overline{\alpha}_n(h_1+h_2+h_3)\mu_{2n})\cos(\mu_{2n}) \\ +(\overline{\alpha}_n h_3+\overline{\beta}_n(h_1+h_2+h_3)\mu_{2n})\sin(\mu_{2n}) \end{array}\right)\Big/\mu_{2n}^2 & X_3 \le x \le X_4 \end{cases}. \tag{22}$$

References

[1] V. Zardetto, T.M. Brown, A. Reale, A. Di Carlo, Substrates for flexible electronics: a practical investigation on the electrical, film flexibility, optical, temperature, and solvent resistance properties, J. Polym. Sci. B Polym. Phys. 49 (2011) 638–648.
[2] K. Suganuma, Introduction to Printed Electronics, Springer Science + Business Media, New York, 2014.
[3] K.A. Schroder, S.C. McCool, W.R. Furlan, Broadcast Photonic Curing of Metallic Nanoparticle Films, Tech. Proc. NSTI Nanotechnology Conf. and Trade Show, 32006 198–201.
[4] K.A. Schroder, Mechanisms of Photonic Curing: Processing High Temperature Films on Low Temperature Substrates, Tech. Proc. 2011 NSTI Nanotechnology Conf. and Trade Show, 22011 220–223.
[5] S. Timoshenko, Analysis of bi-metal thermostats, J. Opt. Soc. Am. 11 (1925) 233–255.
[6] B.A. Boley, J.H. Weiner, Theory of Thermal Stresses, Dover Publications, Mineaola, NY, 1988.
[7] G.H. Olsen, M. Ettenberg, Calculated stresses in multilayered heteroepitaxial structures, J. Appl. Phys. 48 (1977) 2543–2547.
[8] H. Shimizu, H.K. Itoh, M. Wada, T. Sugino, I. Teramoto, Improvement in operation lives of GaAlAs visible lasers by introducing GaAlAs buffer layers, IEEE J. Quantum Electron. 17 (1981) 763–767.
[9] Z. Feng, H. Liu, Generalized formula for curvature radius and layer stresses caused by thermal strain in semiconductor multilayer structures, J. Appl. Phys. 54 (1983) 83–85.
[10] H.C. Liu, S.P. Murarka, Elastic and viscoelastic analysis of stress in thin films, J. Appl. Phys. 72 (1992) 3458–3463.
[11] T.J. Lu, N.A. Fleck, The thermal shock resistance of solids, Acta Metall. 46 (1998) 4755–4768.
[12] J. Malzbender, R.W. Steinbrech, Mechanical properties of coated materials and multi-layered composites determined using bending methods, Surf. Coat. Technol. 176 (2003) 165–172.
[13] J. Malzbender, Mechanical and thermal stresses in multilayered materials, J. Appl. Phys. 95 (2004) 1780–1782.
[14] X.C. Zhang, B.S. Xu, H.D. Wang, Y.X. Wu, An analytical model for predicting thermal stresses in multilayer systems, Thin Solid Films 488 (2005) 274–282.
[15] X.C. Zhang, B.S. Xu, H.D. Wang, Y. Jiang, Y.X. Wu, Modeling of thermal residual stresses in multilayer coatings with graded properties and compositions, Thin Solid Films 497 (2006) 223–231.
[16] A.G. Evans, J.W. Hutchinson, The mechanics of coating delamination in thermal gradients, Surf. Coat. Technol. 201 (2007) 7905–7916.
[17] L.B. Freund, The stress distribution and curvature of a general compositionally graded semiconductor layer, J. Cryst. Growth 132 (1993) 341–344.
[18] L.B. Freund, Some elementary connections between curvature and mismatch strain in compositionally graded thin films, J. Mech. Phys. Solids 44 (1996) 733–736.
[19] A.E. Giannakopolous, S. Suresh, M. Finot, M. Olsson, Elastoplastic analysis of thermal cycling: layered materials with compositional gradients, Acta Metall. Mater. 43 (1995) 1335–1354.
[20] C.H. Hsueh, Thermal tresses in elastic multilayer systems, Thin Solid Films 418 (2002) 182–188.
[21] N.H. Zhang, Thermoelastic stresses in multilayer beams, Thin Solid Films 515 (2007) 8402–8406.
[22] X. Feng, Y. Huang, A.J. Rosakis, Stresses in multilayer thin film/substrate system subjected to nonuniform temperature, J. Appl. Mech. 75 (2008) 021022-1–021022-7.
[23] S. Sundaram, D.M. Lipkin, C.A. Johnson, J.W. Hutchinson, The influence of transient thermal gradients and substrate constraint on delamination of thermal barrier coatings, J. Appl. Mech. (2013) 011002-1–011022-13.
[24] M.J. Guillot, K.A. Schroder, S.C. McCool, Simulating the thermal response of thin films during photonic curing, Paper. IMECE2012-7674, Proc. ASME 2012 IMECE, V7: Fluids and Heat Transfer, Parts A, B, C, D 2012, pp. 19–27.
[25] M.J. Guillot, S.C. McCool, Effect of boundary condition approximation on a finite volume discretization of the transient heat conduction approximation for several benchmark cases, Int. J. Numer. Methods Heat Fluid Flow 25 (2015) 950–972.
[26] J.V. Beck, Heat Conduction using Greens Functions, Hemisphere Publishing, London, 1992.
[27] Y. Sun, I.S. Wichman, On transient heat conduction in a one-dimensional composite slab, Int. J. Heat Mass Transf. 47 (2004) 1555–1559.
[28] David R. Lide, Editor in Chief, CRC Handbook of Chemistry and Physics, 85th ed., CRC Press, Boca Raton, 2004.